1981-06-01

Molecular dynamics simulation study of the influence of the ion mass upon atom ejection processes

Harrison, D.E. Jr.

American Institute of Physics

Journal Name: J. Appl. Phys.; (United States); Journal Volume: 52:6
https://hdl.handle.net/10945/60954

A molecular dynamics simulation study of the influence of the ion mass upon atom ejection processes

Don E. Harrison, Jr.
Department of Physics and Chemistry, Naval Postgraduate School, Monterey, California 93940

(Received 2 December 1980; accepted for publication 4 March 1981)

A molecular dynamics simulation has been used to investigate the ion mass dependence of single-crystal atom ejection. Atom yield ratios, surface damage cross sections, atoms ejected per single ion (ASI) distributions, ejected atom energy distributions, layer yield ratios, and multimer yield ratios have been computed for normally incident Ne, Ar, Cu, Kr, and Xe ion masses on Cu targets for two very different Born-Mayer ion-atom potential functions. Results are compared with experimental data where feasible. The sputtering yield is found to increase with the ion size, as fixed by the ion-atom potential function, not with the ion mass. Experimental ejected atom energy distribution functions should show an ion mass dependence at higher atom energies. The layer yield ratios decrease as the ion mass increases. The heavier ions show no increased tendency to eject clumps of material or to create large, deep craters in the target surface. Atoms driven into the target may make a significant contribution to near-surface depleted zones and crater formation. The multimer yield ratios show very little ion mass dependence. ASI distributions and surface layer damage distributions show how momentum changes at constant ion energy affect the sputtering dynamics.

PACS numbers: 79.20.Nc, 34.20.Be, 61.80.Jh

The results reported here are an outgrowth of the author's molecular dynamics simulations, and were motivated by concerns about the choice of appropriate parameters for use in this work. For many years, most of our classical trajectory simulation investigations of sputtering and other atom ejection phenomena have been carried out on the Cu/Ar^+ system.[1] References which describe the details of the model are indicated by an asterick in the footnotes. Adatoms of other elements have been introduced,[2] and some investigations have been done on Ni targets,[3] but Cu/Ar^+ has been the base system. Other authors, using quite different computational models,[4] have examined other systems, usually with some variation on the Moliere potential function.

The first paper of the present series,[5] which will be referred to as IAP, addressed the potential selection problem by varying only the ion-atom interaction function. The ion mass and all parameters associated with the target were held constant. This paper reports in a similar fashion on an investigation of ion mass changes. Only two potential functions will be used, and again, all target parameters will remain fixed. This approach makes it possible to separate effects caused by variation of the mass from other effects produced by changes in the ion-atom potential function.

This type of parameter variation makes direct comparison with experiment difficult, but not impossible. In fact, one experimental result discussed here supports the central result of IAP: that if the magnitude of the ion-atom potential is known in a sensitive separation range (SSR) around 1.0 Å; then the sputtering properties of the system can be predicted quite accurately from other simulation calculations.

Details of the classical dynamics procedure have been described elsewhere.[1,6] Hamilton's equations of motion are solved in time for an incoming ion and a four-layer microcrystallite containing ~90 atoms/layer. Target orientation is determined by the original locations of the lattice atoms. These atoms interact through a compound potential formed from a Gibson II wall and an Anderman well joined with a cubic spline.[1] To minimize channeling effects the computations reported here were all performed on the (111) orientation of the target crystal. The ion is aimed toward an impact point in an irreducible symmetry zone of the target surface, and the resultant collision cascade, or trajectory, continues until the remaining atoms have insufficient energy to escape the surface. Energy losses to electronic excitations have not been included in this particular computation. Global values, required for direct comparison with experiment, are obtained by averaging over results from 80 trajectories done with a set of impact points which are uniformly distributed over the impact zone. Care has been taken to keep the program computationally identical to the model used in the first paper of this series.[15] Numerous physical and computational aspects of the model have recently been summarized.[7]

The calculations discussed here were made with a family of five ions: Ne, Ar, Cu, Kr, and Xe, which span across mass ratios ($m_i/m_j = m_1/m_2$) from 0.3176 to 2.066 when used with Cu targets. Where direct comparison is made with experiment both the computed and measured results will be normalized to the same value, so that the variations can be displayed more prominently.

Most of the computations in IAP were performed with Born-Mayer potential functions

$$V(r) = A \exp(-br).$$

The parameter b is the slope of the function on a semi-logarithmic plot. Here results will be reported for the B and R potential functions which are discussed in detail in that paper. Their parameters are listed in Table I. In these computations the lattice atoms are always Cu, so it is convenient when discussing results to associate the properties of the potential function with the ion: the R potential produced a

TABLE I. These are the parameters of the Born-Mayer ion-atom potential functions used for the computations of this paper. These functions span the possible ion-atom interactions from very small and soft to very large and hard. The reasons for this particular choice are given in IAP.[5]

potential function	A (KeV)	$a = \ln A$	B (Å^{-1})
B	71.303	11.174	−4.593
R	59.874	11.000	−7.200

small ion and B a large ion, because R has a much larger slope than B. Similarly, B is much harder than R, because its pre-exponential constant A is greater than R's. This assignment has no effect on the actual computations.

YIELD RATIO

Figure 1 shows the computed (111) orientation *yield ratios* Y/Y_{Ar}, at three ion energies for one potential function and two energies for the other. Similarly normalized experimental yield ratios, computed from the single-crystal yield data of Onderdelinden,[8] have been included where they exist. In addition to his own work, he summarizes data from Southern, Willis, and Robinson[9] and Magnuson and Carlston.[10] The 600-eV points are taken from his extrapolations. The polycrystalline target results reported by Laegreid and Wehner[11] also are almost mass independent, and have similar values at this energy.

At low ion energy the ion mass dependence of the yield ratio is potential function sensitive. For the very small R potential ion the yield ratio decreases as the ion mass increases; for the large B potential ion it is effectively constant. At 5.0 KeV the two potentials give essentially the same results. The 5.0 and 10.0-KeV B potential curves are almost identical. The computed curve follows the experimental points at low energy, but deviates strongly at higher energy. This figure shows that *the experimental increase of yield with increasing ion mass is not a mass effect*! It can be attributed to an increase in ion size as Z_1 the ion atomic number increases. This yield increase with size has been discussed in IAP.

At 600 eV, both the computed and experimental yield ratios are almost independent of the ion mass. At this low energy the ion probes only the more distant portion of the potential funciton. Large impact parameter collisions do not contribute because they are dominated by other, harder collisions; so these three ion-atom potential functions must be similar at separations near 1.0 Å. The data support the conclusion of IAP that the sputtering yield depends most strongly on the magnitude of the ion-atom potential function in this sensitive separation range. The detailed argument is presented in IAP.

SURFACE LAYER DAMAGE CROSS SECTION

The total yield does not illustrate the strong mass dependence of sputtering processes. The dynamics do change significantly as the ion mass increases, and the first layer damage cross sections are quite different. These effects can be seen in the ejection probabilities for atoms at different distance from the target atom. This sort of microscopic information cannot be confirmed experimentally, but it helps with the interpretation of experimental results.[12]

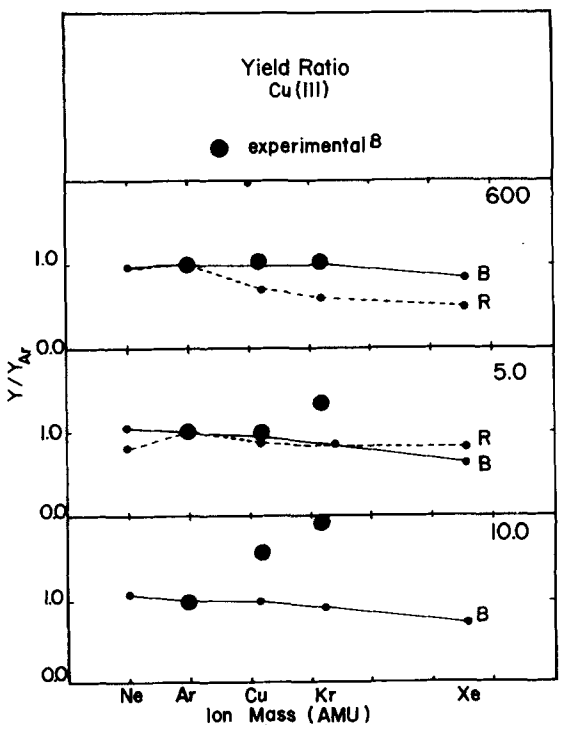

FIG. 1. Comparison of the yield ratios (defined in the text) computed with the two ion-atom potential functions at 600 eV, 5.0 KeV, and 10.0 KeV to the experimental yield ratios obtained from Onderdelinden.[8] The agreement is excellent at low energies. The divergence at higher ion energy shows that that experimental yield ratio changes are not caused by the change in ion mass.

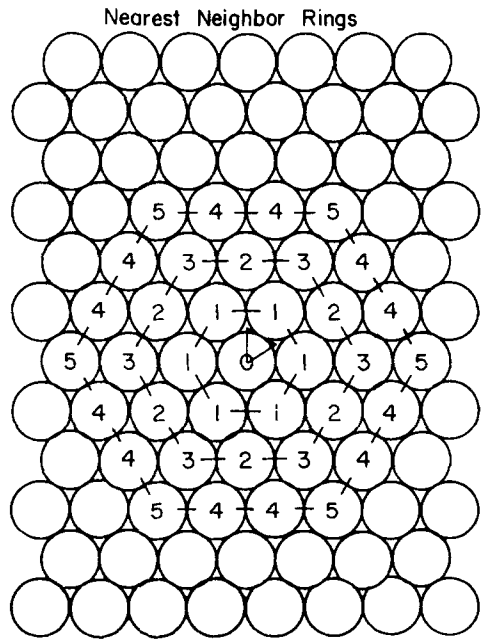

FIG. 2. Picture of the top layer of the target microcrystallite used in these computations. The first three rings of neighboring atoms and the target atom are indicated. The triangle is the impact zone. The fourth ring is not shown. See the text for a detailed discussion of the use of this description of the surface damage cross section.

the interpretation of experimental results.[12]

On the (111) surface rings are easily drawn around the target atom, see Fig. 2. The ion impact zone is indicated by the triangle. To simplify the presentation, the target atom is called ring zero. The first ring consists of the six nearest-neighbor, NN(1), atoms in the surface layer. The second ring contains six NN(2) and six NN(3) atoms, the third ring twelve NN(4) and six NN(5) atoms, and the fourth ring (not shown in the figure) eighteen NN(6) and six NN(7) atoms. The actual target is two atoms short in the fourth ring, but sample calculations with larger targets confirm that the probabilities of ejection for the two omitted atoms are comparable to these reported here.

The probability of ejection for each atom is the number of times it is ejected, divided by the number of trajectories in the sample. These probabilities have been averaged for each ring. Yield fractions for each ring can be obtained by multiplying the probabilities by 6 for ring 1, 12 for ring 2, 18 for ring 3, and 24 for ring 4.

Results for the two potential functions are shown in Figs. 3 and 4. The B potential results are less scattered because the computed yields are much larger.

For the large ion potential B, the ejection probabilities are plotted against the mass, for each ring. For mass ratios < 1.0, the probability of ejection for the target atom, ring 0, increases with the ion energy and decreases with ion mass. At 600 eV the maximum probability of ejection moves outward from ring 1 to ring 2 as the mass increases because the heavier ions increasingly force the first ring atoms down. The second ring probabilities increase because the recoiling first ring atoms are passing under them. The third ring probabilities are lower than the second because of the up-down mechanism.[1]

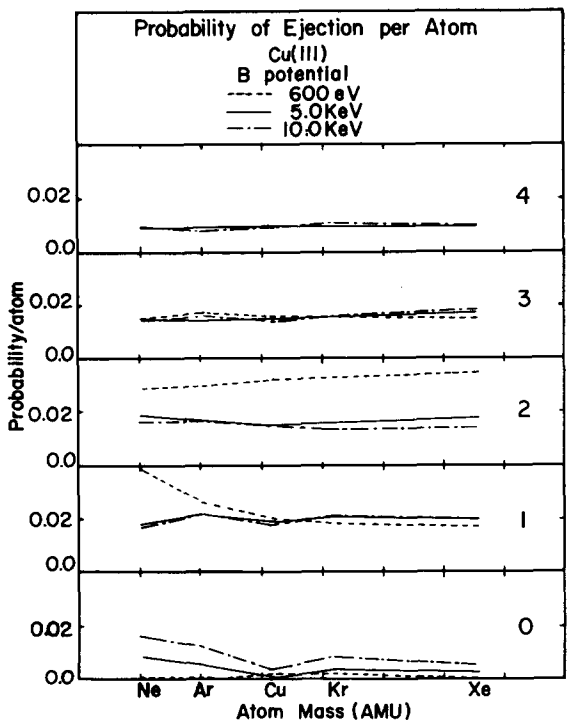

FIG. 3. B potential probabilities of ejection for the atoms of each ring are plotted for the target atom, ring 0, and the four rings of neighboring atoms. This presentation emphasises the mass dependence of the probabilities, compare Fig. 4. The curves are discussed in detail in the text.

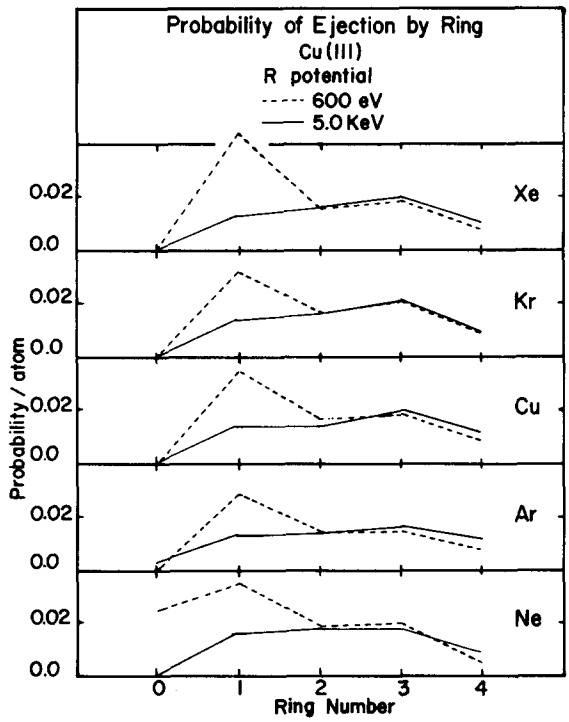

FIG. 4. Shown are the R potential probabilities of ejection for the masses, plotted against the ring number. This presentation emphasises the ring dependence of the probabilities for the individual ions, compare Fig. 3. The curves are discussed in detail in the text.

At higher energies the yield probabilities maximize at the first ring except for Ne, and are nearly mass independent. Above the maximum the yield probability decreases for rings 2 and 3, but more slowly for Xe than for the lighter ions. Most of the atoms are ejected from the second and third rings because they contain many more atoms than the first ring. As the ion mass increases the damage area increase becomes very evident.

This figure demonstrates the importance of momentum effects in sputtering. At constant energy, the ion mass influences the sputtering dynamics only through differences in the momentum transferred. A light ion is easily deflected. It tends to push its primary knock-on atom (PKA) targets sideways, so that they have a fair chance of ejection. A heavy ion has more forward momontum, so it is deflected less by collisions. Atoms which interact with it directly acquire more forward momentum and tend to be driven into the crystal, where they then pass under and eject more distant atoms.

In Fig. 4 the small ion ejection probabilities are plotted for each ion mass as a function of ring number. At 600 eV the yield probabilities maximize at ring 1, and there may be some up-down effect for the heavier ions. At 5.0 KeV the maximum moves outward, reaching ring 3 for mass ratios greater than 1.0. This differs from the B potential results where the ejection probability curves are almost identical for mass ratios > 1.0.

At any energy, the difference in size between the B and R potentials translates into different scattering angles at a

given impact parameter. The transferred momentum is quite different, even when the ion energy and mass are the same. The difference in results for the two potential funcitons demonstrate the influence of the momentum transfer processes, but the persistence of forward momentum effect is dominant.

ASI DISTRIBUTIONS

The experimental yield is not always a good indicator of ejection processes because it is averaged over many ion trajectories. The computer makes it possible to determine a distribution of *atoms ejected per single ion* (ASI).[7,13] Although some of the current investigations of crater formation [14–16] and beginning to supply similar information, this distribution still cannot be determined experimentally. Figure 5 shows the ASI distributions for the five masses and the *B* potential function at 600 eV and at 5.0 KeV. The curves were constructed from 80 trajectory samples, so any single value has high uncertainty, but studies with much larger samples[13] have shown that small samples represent general trends very well. Experience has shown that the maxima of these distributions are not reliable. Larger samples tend to produce maxima at slightly higher values, but the 25th, 50th, and 75th percentile points of the distribution rarely shift by even one atom/ion.[7]

At 600 eV, the distribution is effectively mass independent. There is no reason to believe that any of the differences are significant. At 5.0 KeV the curves indicate that large ASI values are more likely for small ion masses than for large.

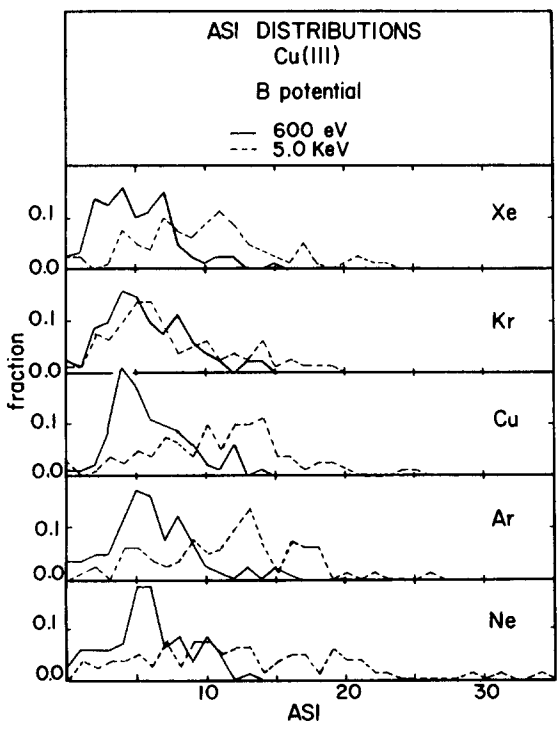

FIG. 5. These curves are the *B* potential atoms/single ion (ASI) distributions at 600 eV and 5.0 KeV. They demostrate the shift of the maximum toward higher values as the ion energy increases, and the increased probability of large ASI values for small ion masses. Note that the large ion ASI = 0 probability is quite small for all ion masses.

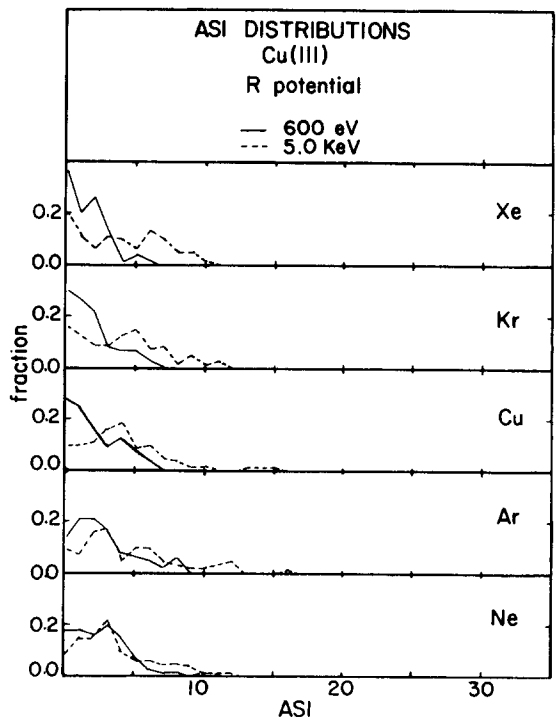

FIG. 6. This repeats Fig. 5 for the *R* potential. With this potential the probability that ASI = 0 is high for all ions, but decreases as the ion mass decreases or the ion energy increases. Total yields are much smaller for the *R* potential, so direct comparisons between Figs. 5 and 6 are difficult. See the text for a detailed discussion.

The maximum in the ASI curve, although not well resolved in Fig. 5, is expected to move toward smaller ASI values as the ion mass increases. This would be consistent with the increased forward momentum of the heavier ions. Examination of individual trajectories indicates that the decrease occurs because the ion recoil angle from the first collision decreases as the ion mass increases. This behavior tends to decrease the transverse momentum transfer to the second PKA, which reduces its contribution to the ASI yield. Some heavy ions trajectories eject many atoms, but the most probable yield decreases.

The same results are shown in Fig. 6 for the *R* potential. Some of the differences between the two potentials reflect the much smaller ions, at 600 eV, the curves peak more strongly at ASI = 0 as the mass increases. At 5.0 KeV a larger fraction of the ions produce some yield for all masses, so the most probable yield is no longer zero. Still, large ASI values become less likely as the ion mass increases.

Figure 7 repeats the *B* potential results at 5.0 KeV so that they can be compared with the 10.0-KeV curves. For each mass the distribution functions have almost the same shape at the two energies. Once again, heavy ions appear less likely to produce large ASI values. Note that all masses have some ASI = 0 trajectories at 10.0 KeV, and the probability of zero yield increases with the ion mass. This is an increase in lattice transparency as the forward momentum increases, not a channeling effect. At these energies the distributions are very broad with this potential function, and many of the individual cascades must by very different from the ensemble average behavior. The *R* potential distributions are nar-

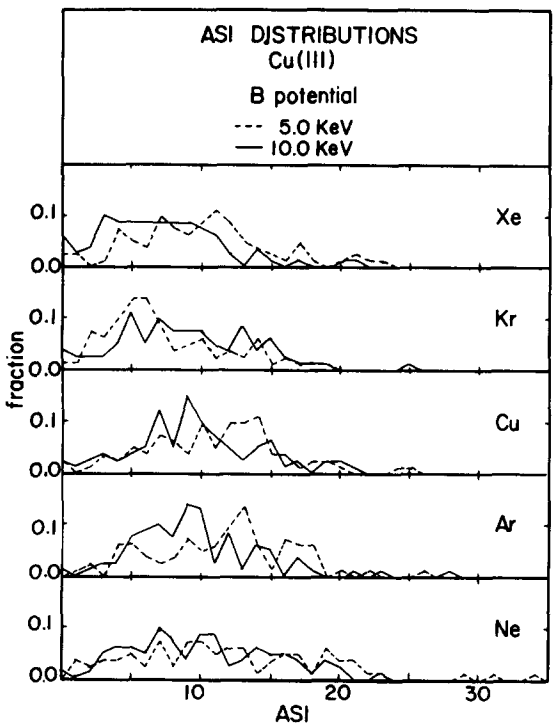

FIG. 7. This figure, for the *B* potential, repeats the 5.0-KeV curve from Fig. 5 so that it can be compared with the 10.0-KeV curve. The maximum ASI values at 10.0 KeV appear to be smaller than at 5.0 KeV. This is consistent with the decrease in yield observed fro Cu/Ar^+ at energies above 5.0 KeV. The curves are discussed in detail in the text.

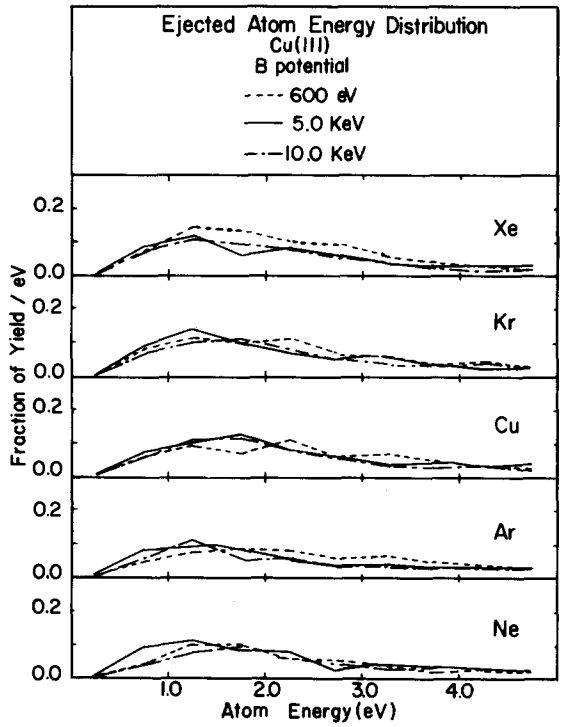

FIG. 8. Shown is the peak of the ejected atom energy distribution functions for the *B* potential at three different energies. The curves are indistinguishable, which indicates that these distributions are dominated by the atom-atom interactions.

rower, and for the heavier ions at 5.0 KeV they have become almost bimodal.

EJECTED ATOM ENERGY DISTRIBUTIONS

Ion mass generated differences are not obvious in the ejected atom energy distributions, whose maxima are shown in Figs. 8 and 9. These distributions are strongly influenced by atom-atom collisions which tend to average out differences introduced by the ions. The *B* potential curves, Fig. 8, are effectively identical at all masses and energies. Once again, because the *R* potential samples are smaller, the curves in Fig. 9 are more difficult to interpret. For heavy ions there is some indication that the maximum of the distribution moves toward a lower evergy as the ion energy increases, but the interpretation is uncertain. This difference for the *R* potential, if significant, depends on the fact that a small ion is more likely to eject atoms near the target atom than more distant ones, so the atom-atom collisions have less influence.

The samples are too small to draw distribution functions, but some information about the high-energy ejected atoms is shown in Figs. 10 and 11. The trends show that high-energy atom ejection becomes less probable as the ion mass increases. At 600 eV only the lightest ions can produce ejected ions with energy greater than 100.0 eV. As high-energy ejections occur early in the cascade, these ejections are determined by ion-atom collisions where the ion mass has a direct influence. The effect is independent of the potential function so long as the ion energy is not too large and the definition of high energy for an ejected atom is a fairly large fraction of the ion energy.

At 600 eV, examination of individual trajectories and probabilities of ejection for individual atoms shows that almost the same atoms are ejected with high energy, regardless

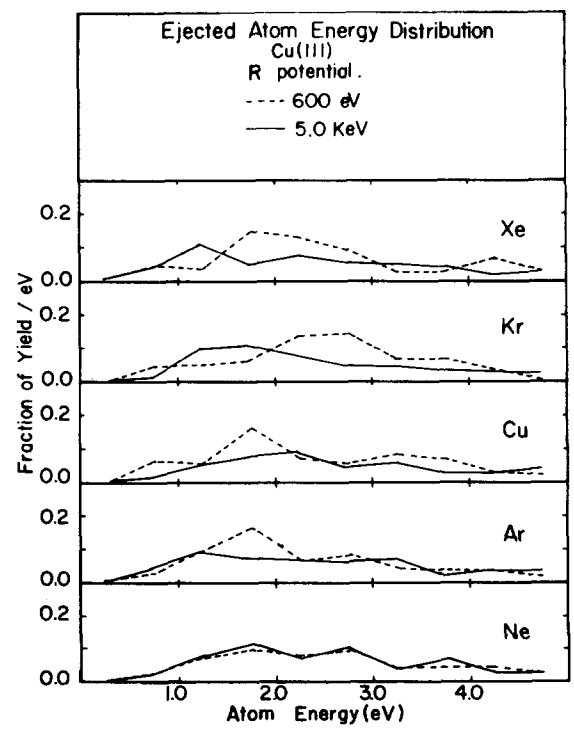

FIG. 9. This repeats Fig. 8 for the *R* potential. The differences in the curves are probably not statistically significant. We conclude that the ion mass has little effect on the maximum region of the ejected atome energy distribution.

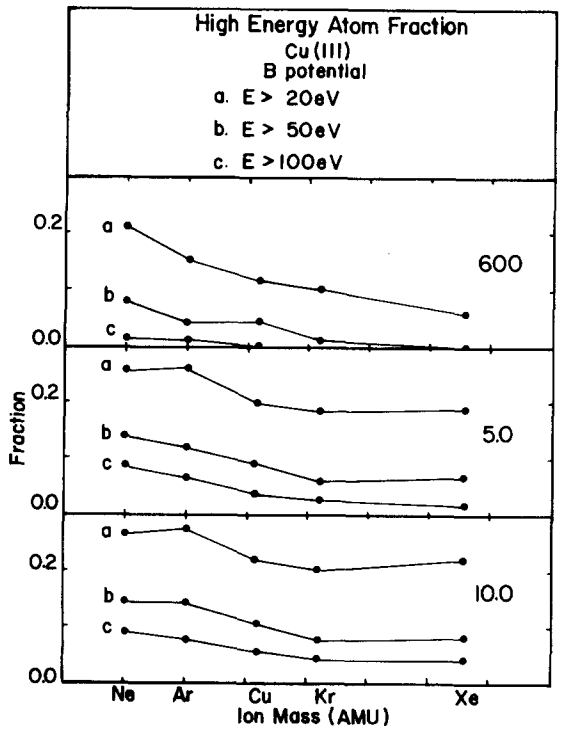

FIG. 10 Shown is the fraction of ejected atoms with energy exceeding the indicated value for the *B* potential and each ion mass at 600 eV, 5.0 KeV, and 10.0 KeV. The 50-eV and 100-eV curves all show a decrease as the ion mass increases. The 20-eV curve shows the decrease at 600-eV ion energy, but is less clear cut at higher ion energies. This is a direct demostration of the infuence of momentum transfer effects in atom ejection, and may be detectable in experimental ejected atom energy distribution data when they becom available. Unfortunately, a family of curves of this type does not exist at present.

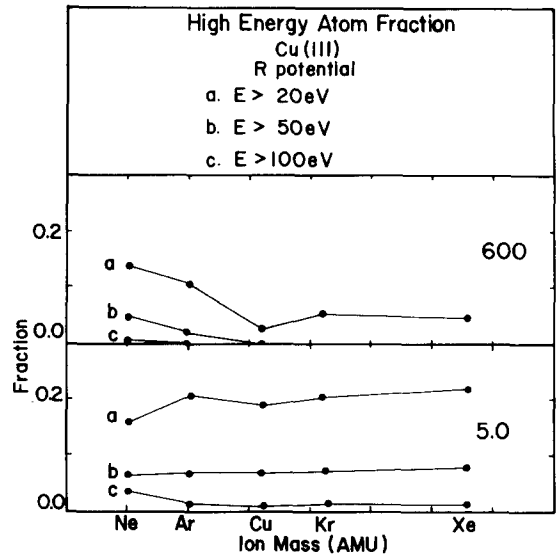

FIG. 11. This provides the same information as Fig. 10 for the *R* potential, at 600-eV and 5.0-KeV ion energies. The decrease in high-energy atom fraction with increasing ion mass in apparent at 600 eV, and in the 100-eV curve at 5.0 KeV. The difinition of a high-energy ejected atom is clearly dependent upon the nature of the ion-atom potential function, because the (a) and (b) curves do not show the effect at 5.0 KeV. It may be possible to obtain some information about the ion-atom potential function from this type of experiment.

of the ion mass. The dynamical processes must be very similar, but as the ion mass increases the energy transferred to the first layer PKA's decreases, so even the most favorably placed high-energy ejected atoms receive less energy.

LAYER YIELD RATIOS

MCI collision model studies of the Cu/Ar^+ system[5,7] predict that most of the ejected atoms come from the surface layer of the target. Second layer yields rarely exceed 10% of the total, and the third layer contribution is roughly another factor of 10 smaller. This behavior has been reported for a wide range of ion-atom potential functions, and a single mass ratio. *Layer yield ratios* $L_n = N_n/N$ (where N_n is the number of atoms ejected from the nth layer of the target and N is total number of atoms ejected) are a convenient way to present these data.

In an attempt to explain the extremely large atom yields observed for diatomic and triatomic molecular ions of heavy atoms Thompson[17] has proposed a model that depends on the formation of very large surface craters by almost every ion. Craters of this type are similar to the "near-surface depleted zones"studied by Current and Seidman,[14] but their experiments suggest that large craters may be rare events. As a further contribution to this unresolved issue, the mass dependence of the layer yield ratios for the two potentials are shown in Fig. 12 and 13.

At 600 eV there is no third layer yield with any ion mass from either potential function. The second layer yield ratio is essentially constant for the *B* potential, and decreases with increasing ion mass for the *R* potential. At higher energies

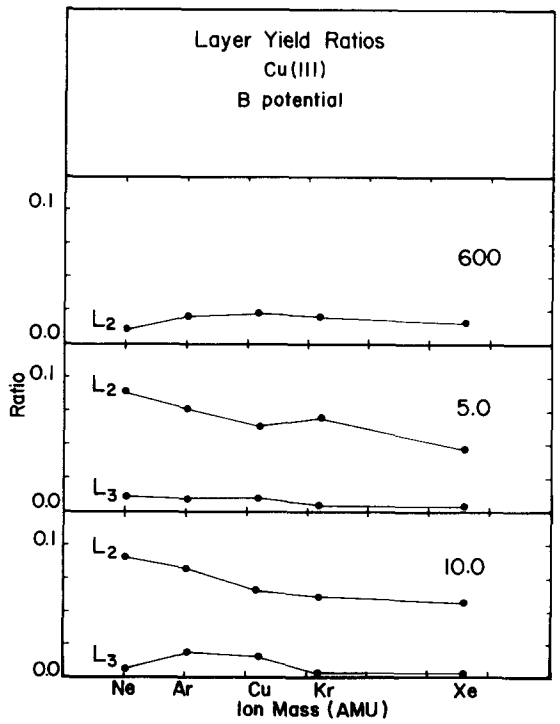

FIG. 12. Layer yield ratios are the fractions of the ejected atoms whose original site was in the second or third atomic layer of the target. These curves, drawn for the *B* potential, show that second and third layer yield fractions decrease as the ion mass increases. This behavior suggests that heavy ions should not form deep craters. The consequences of this finding are discussed in the text.

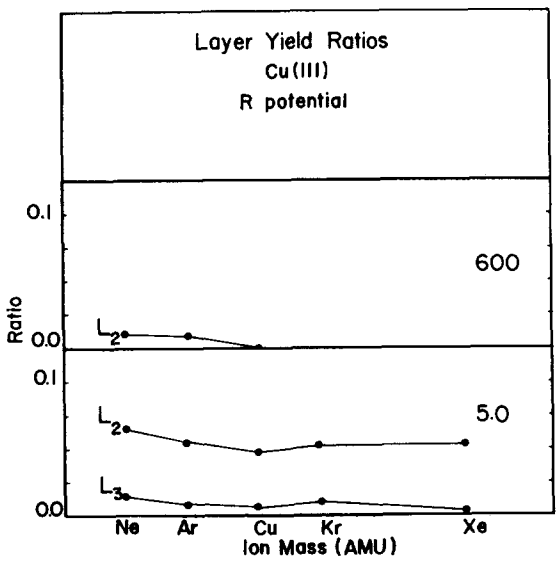

FIG. 13. Shown are curves similar to those in Fig. 12 for the *R* potential. The behavior is the same, so evidently the layer yield ratio decrease with ion mass is not sensitive to the ion-atom potential function.

the layer yield ratios decrease as the ion mass increases. None of the individual numbers is very reliable, because they are obtained from small atom counts, but the trends are quite clear. At constant energy, as the ion mass increases the relative number of atoms ejected from the second and third layers decreases. Energy dependence studies of the simulation have not been reported in great detail,[7] but the (111) and (001) layer yield ratios for Cu/Ar^+ have broad maxima between 5.0 and 10.0 KeV.[7] L_2 falls off more rapidly than L_3 above 10.0 KeV, but both are clearly declining. This behavior is not potential function dependent.

For the *B* potential, the computations seem to indicate that the layer yield ratio maxima move toward higher energy as the ion mass increases, compare Ar and Xe, for example. More points, with larger samples, would be required to be certain. 5.0 KeV is not high enough to give this information for the *R* potential.

There is no evidence that an increase in the ion mass increases the probability that events occurring below the crystal surface will be reflected by detectable changes at the surface, or that a further increase in ion energy would significantly increased the yield from lower layers. Large patches of the surface layer could still be ejected, but there is no support for a model which requires that almost every ion must dig a deep crater.[17]

The crater analysis experiments referred to earlier[14] differ from the computations in two important respects: they determine the final state of the target (but give no information about the sites from which the atoms were ejected or their final positions), and the experiments were done at somewhat higher ion energies.

In principle the computer could follow the cooling of the target after the trajectory is complete and predict the characteristics of the final craters, but these computations have not yet been done. The computations do produce one effect which might not be anticipated from the data: many atoms from the impact region are driven into the crystal with relatively high energy. They will become stable interstitials which cannot relax back into the crater. The corresponding vacancies may actually make a larger contribution to the final crater size than the ejected atoms.

MULTIMER YIELD RATIOS

Multimer yield ratios measure the fraction of ejected atoms which come away from the surface as molecular clusters.[1] The *dimer/monomer ratio* $M_2 = Y_2/Y_1$ and the *trimer/monomer ratio* $M_3 = Y_3/Y_1$ computed in simulations compare very favorably with the ratios for molecular ions as measured in a SIMS system.[18] The ion mass dependence of these ratios for the two potential functions is shown in Figs. 14 and 15. At 600 eV for the *B* potential M_2 may by increasing with the ion mass, but there is no certainty, because the dimer yields are small. None of the other curves has a defensible trend.

Multimers occur more frequently in large ASI trajectories;[19] so the total yield is not a good predictor of multimer yields.[20,21] For Cu/Ar^+ the multimer yield ratios fall off at energies above 10.0 KeV, but here there are insufficient data to confirm similar behavior. These results are consistent with the Cu/Ar^+ data which indicate very strongly that the multimer yield ratios are fixed by the atom-atom interactions, and are little influenced by changes in the ion-atom function.[5] Had the layer yield ratios been significantly mass sensitive a mass effect might have been detected in the multimer ratios, but this is not the case.

Unfortunately, the data are not available which would allow a direct comparison with experiment. Because these

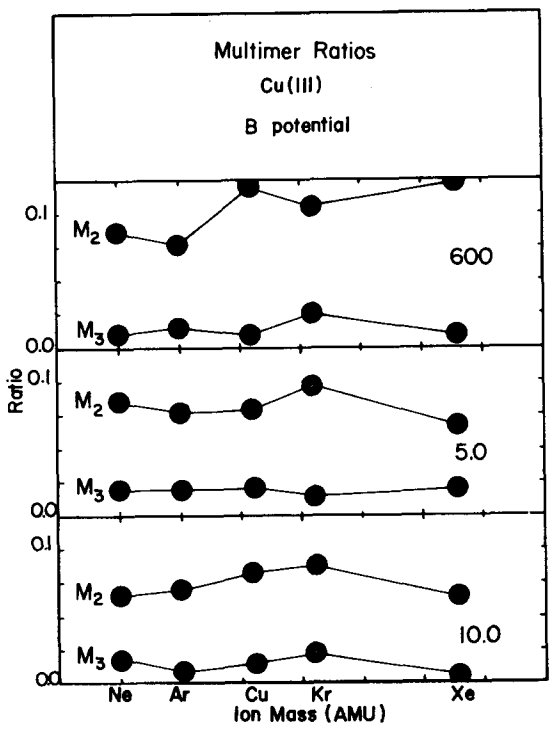

FIG. 14. Multimer yield ratios are defined in the text. For the *B* potential they do not show any strong dependence on the ion mass at any of the three energies examined. This agrees with other evidence that multimer formation is primarily the result of atom-atom collisions.

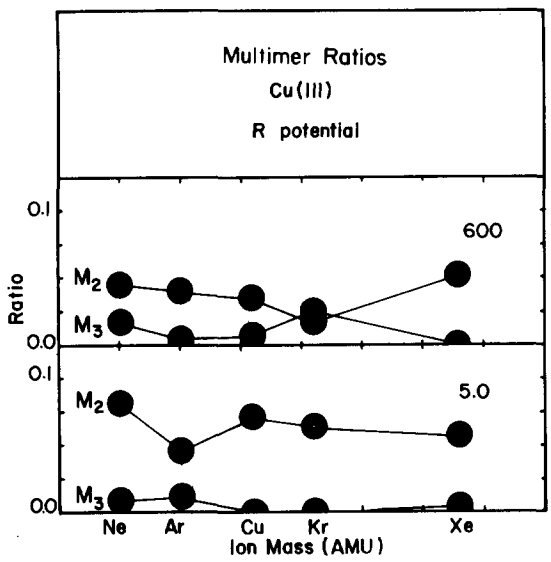

FIG. 15. Multimer yield ratio curves for the R potential function. The total multimer yields are small for this function so the uncertainty of each point is high. The crossing of the M_2 and M_3 curves at 600 eV demonstrates this uncertainty. At low ion energy the R potential ratios are lower than the B potential ratios, but neither differs greatly from the experimental ratios obtained by SIMS for molecular ions.

ratios are almost independent of total yield as it changes with potential function at constant ion energy, one might hope to find a similar independence of ion mass. SIMS experiments, using the molecular ions would be helpful, although an additional process, ionization, has been introduced.

SUMMARY AND CONCLUSIONS

Although this investigation began from the unrealistic premise that it is possible to change ion masses without changing the ion-atom potential function, it does produce some results which are of interest, and some of the conclusions may be confirmable by experiments.

(1) The experimentally detectable increase of relative yield with the ion atomic number is an ion size effect, not a mass effect.

(2) Analytic sputtering theories,[22] which do not emphasize momentum effects directly, give good predictions of the total yield. More subtle experiments, such as examination of the high-energy portion of the ejected atom energy distribution, may be able to detect persistence of forward momentum and momentum transfer effects. Mass effects will be most evident at low ion energies where the PKA collision effects are not drowned out by atom-atom collision events.

(3) The location of the peak of the ejected atom energy distribution function is not shifted by changing the ion mass, which indicates that these most probable atom ejections are dominated by atom-atom collision processes.

(4) The surface damage produced by an individual ion is quite mass sensitive. As one would expect, heavier ions produce more widespread damage. The effect of a momentum increase by mass change at constant energy differs from the effect at constant mass and increased energy. This confirms that surface analysis by ion bombardment techniques, SIMS for example, should be accomplished with the lightest possible ion the lowest feasible ion energy.

(5) Heavy ions tend to produce atom yield from broad regions, but the ejection depth is independent of the ion mass. There is no indication that craters become deeper as the ion energy increases.

(6) Calculated multimer yield ratios provide further evidence that multimers are produced primarily by atom-atom processes.

These computations suggest that ion mass effects can be found in detailed atom ejection experiments, but that they are not so important as one might presume from the study of two-body collisions. Great care must be taken in the analysis of experimental or computational results if ion size (potential function) and ion mass effects are to be separated.

ACKNOWLEDGMENTS

This investigation was supported by the Structural Chemistry and Thermodynamics Program of the National Science Foundation and by the Office of Naval Research throught the Foundation Research Program of the Naval Postgraduate School.

[1]D. E. Harrison, Jr., W. L. Moore, Jr., and H. T. Holcombe, Radiat Eff. **17**, 167 (1973)*; D. E. Harrison, Jr. and C. B. Delaplain, J. Appl. Phys. **47**, 2252 (1976); D. E. Harrison, Jr., P. W. Kelly, B. J. Garrison, and N. Winograd, Surf. Sci. **76**, 331 (1978)*; B. J. Garrison, N. Winograd, and D. E. Harrison, Jr., J. Chem. Phys. **69**, 1440 (1978).
[2]B. J. Garrison, N. Winograd, and D. E. Harrison, Jr., Phys. Rev. B **18**, 6000 (1978)*.
[3]S. P. Holland, B. J. Garrison, and N. Winograd, Phys. Rev. Lett. **44**, 756 (1980).
[4]J. P. Biersack and L. G. Haggmark, J. Nucl. Mater. **93–94** Pt B, 664 (1980); Nucl. Instru. Methods **174**, (1) 257 (1980).
[5]D. E. Harrison, Jr., J. Appl. Phys. **52**, 1499 (1981).
[6]D. E. Harrison, Jr., W. L. Gay, and H. M. Effron, J. Math. Phys. **10**, 1179 (1969).
[7]See D. E. Harrison, Jr., Full Lattice Simulation of Atom Ejection Mechanisms and Sputtering, Proceedings of the Symposium on Sputtering, edited by P. Varga, G. Betz, and F. P. Viehbock, Perchtoldsdorf/Vienna, 1980, pp. 36–61 (unpublished)*.
[8]D. Onderdelinden, Can. J. Phys. **46**, 739 (1968).
[9]A. L. Southern, W. R. Willis, and M. T. Robinson, Phys. Rev. **A139**, 737 (1965).
[10]G. D. Magnuson and C. E. Carlston, J. Appl. Phys. **34**, 3267 (1963).
[11]N. Laegreid and G. K. Wehner, J. Appl. Phys. **32**, 365 (1961).
[12]K. E. Foley and B. J. Garrison, J. Chem. Phys. **72**, 1018 (1980).
[13]D. E. Harrison, Jr., B. J. Garrison, and N. Winograd, *Secondary Ion Mass Spectrometry SIMS II*, edited by A Benninghoven, C. A. Evans, Jr., R. A. Powell, R. Shimizu, and H. A Storms (Springer, New York, 1979), p 12.
[14]M. I. Current and D. N. Seidman, Nuc. Instrum. Methods **170**, 377 (1980).
[15]J. Aidelberg and D. N. Seidman, Nucl. Instrum. Methods **170**, 413 (1980).
[16]M. I. Current, C. Y. Wei, and D. N. Seidman, Philos. Mag. **A43**(1), 103 (1981).
[17]See D. A. Thompson, Non-Linear Effects in Sputtering, Proceedings of the Symposium on Sputtering, edited by P. Varga, G. Betz, and F. P. Viehbock, Perchtoldsdorf/Vienna, 1980, pp. 62–100 (unpublished); J. Appl. Phys. p **53**, 982 (1981).
[18]N. Winograd, B. J. Garrison, T. Fleisch, W. N. Delgass, and D. E. Harrison, Jr., J. Vac. Sci. Technol. **16**, 629 (1979).
[19]N. Winograd, D. E. Harrison, Jr., and B. J. Garrison, Surf. Sci. **78**, 467 (1978).
[20]N. Winograd, K. E. Foley, B. J. Garrison, and D. E. Harrison, Jr., Phys. Lett. **A73**, 253 (1979).
[21]K. Wittmaack, Phys. Lett. **A69**, 322 (1979).
[22]P. Sigmund, Phys. Rev. **184**, 383 (1969).